

1 **Observations of the young Supernova remnant RX J1713.7–3946**
 2 **with the *Fermi* Large Area Telescope**

3 A. A. Abdo², M. Ackermann^{3,1}, M. Ajello³, A. Allafort³, L. Baldini⁴, J. Ballet⁵,
 4 G. Barbiellini^{6,7}, M. G. Baring⁸, D. Bastieri^{9,10}, R. Bellazzini⁴, B. Berenji³,
 5 R. D. Blandford³, E. D. Bloom³, E. Bonamente^{11,12}, A. W. Borgland³, A. Bouvier¹³,
 6 T. J. Brandt^{14,15,16}, J. Bregeon⁴, M. Brigida^{17,18}, P. Bruel¹⁹, R. Buehler³, S. Buson^{9,10},
 7 G. A. Caliendo²⁰, R. A. Cameron³, P. A. Caraveo²¹, J. M. Casandjian⁵, C. Cecchi^{11,12},
 8 S. Chaty⁵, A. Chekhtman²², C. C. Cheung²³, J. Chiang³, A. N. Cillis^{24,25}, S. Ciprini¹²,
 9 R. Claus³, J. Cohen-Tanugi²⁶, J. Conrad^{27,28,29}, S. Corbel^{5,30}, S. Cutini³¹, A. de Angelis³²,
 10 F. de Palma^{17,18}, C. D. Dermer³³, S. W. Digel³, E. do Couto e Silva³, P. S. Drell³,
 11 A. Drlica-Wagner³, R. Dubois³, D. Dumora³⁴, C. Favuzzi^{17,18}, E. C. Ferrara²⁵, P. Fortin¹⁹,
 12 M. Frailis^{32,35}, Y. Fukazawa³⁶, Y. Fukui³⁷, S. Funk^{3,1}, P. Fusco^{17,18}, F. Gargano¹⁸,
 13 D. Gasparrini³¹, N. Gehrels²⁵, S. Germani^{11,12}, N. Giglietto^{17,18}, F. Giordano^{17,18},
 14 M. Giroletti³⁸, T. Glanzman³, G. Godfrey³, I. A. Grenier⁵, M.-H. Grondin³⁹, S. Guiriec⁴⁰,
 15 D. Hadasch²⁰, Y. Hanabata³⁶, A. K. Harding²⁵, M. Hayashida³, K. Hayashi³⁶, E. Hays²⁵,
 16 D. Horan¹⁹, M. S. Jackson^{41,28}, G. Jóhannesson⁴², A. S. Johnson³, T. Kamae³,
 17 H. Katagiri³⁶, J. Kataoka⁴³, M. Kerr³, J. Knödseder^{14,15}, M. Kuss⁴, J. Lande³,
 18 L. Latronico⁴, S.-H. Lee³, M. Lemoine-Goumard^{34,44}, F. Longo^{6,7}, F. Loparco^{17,18},
 19 M. N. Lovellette³³, P. Lubrano^{11,12}, G. M. Madejski³, A. Makeev², M. N. Mazziotta¹⁸,
 20 J. E. McEnery^{25,45}, P. F. Michelson³, R. P. Mignani⁴⁶, W. Mitthumsiri³, T. Mizuno³⁶,
 21 A. A. Moiseev^{47,45}, C. Monte^{17,18}, M. E. Monzani³, A. Morselli⁴⁸, I. V. Moskalenko³,
 22 S. Murgia³, M. Naumann-Godo⁵, P. L. Nolan³, J. P. Norris⁴⁹, E. Nuss²⁶, T. Ohsugi⁵⁰,
 23 A. Okumura⁵¹, E. Orlando^{3,52}, J. F. Ormes⁴⁹, D. Paneque^{53,3}, D. Parent², V. Pelassa⁴⁰,
 24 M. Pesce-Rollins⁴, M. Pierbattista⁵, F. Piron²⁶, M. Pohl^{54,55}, T. A. Porter^{3,3}, S. Rainò^{17,18},
 25 R. Rando^{9,10}, M. Razzano⁴, O. Reimer^{56,3}, T. Reposeur³⁴, S. Ritz¹³, R. W. Romani³,
 26 M. Roth⁵⁷, H. F.-W. Sadrozinski¹³, P. M. Saz Parkinson¹³, C. Sgrò⁴, D. A. Smith³⁴,
 27 P. D. Smith¹⁶, G. Spandre⁴, P. Spinelli^{17,18}, M. S. Strickman³³, H. Tajima^{3,58},
 28 H. Takahashi⁵⁰, T. Takahashi⁵¹, T. Tanaka³, J. G. Thayer³, J. B. Thayer³,
 29 D. J. Thompson²⁵, L. Tibaldo^{9,10,5,59}, O. Tibolla⁶⁰, D. F. Torres^{20,61}, G. Tosti^{11,12},
 30 A. Tramacere^{3,62,63}, E. Troja^{25,64}, Y. Uchiyama^{3,1}, J. Vandenbroucke³, V. Vasileiou²⁶,
 31 G. Vianello^{3,62}, N. Vilchez^{14,15}, V. Vitale^{48,65}, A. P. Waite³, P. Wang³, B. L. Winer¹⁶,
 32 K. S. Wood³³, H. Yamamoto³⁷, R. Yamazaki⁶⁶, Z. Yang^{27,28}, M. Ziegler¹³

¹Corresponding authors: M. Ackermann, markusa@slac.stanford.edu; S. Funk, funk@slac.stanford.edu; Y. Uchiyama, uchiyama@slac.stanford.edu.

²Center for Earth Observing and Space Research, College of Science, George Mason University, Fairfax, VA 22030, resident at Naval Research Laboratory, Washington, DC 20375

³W. W. Hansen Experimental Physics Laboratory, Kavli Institute for Particle Astrophysics and Cosmology, Department of Physics and SLAC National Accelerator Laboratory, Stanford University, Stanford, CA 94305, USA

⁴Istituto Nazionale di Fisica Nucleare, Sezione di Pisa, I-56127 Pisa, Italy

⁵Laboratoire AIM, CEA-IRFU/CNRS/Université Paris Diderot, Service d’Astrophysique, CEA Saclay, 91191 Gif sur Yvette, France

⁶Istituto Nazionale di Fisica Nucleare, Sezione di Trieste, I-34127 Trieste, Italy

⁷Dipartimento di Fisica, Università di Trieste, I-34127 Trieste, Italy

⁸Rice University, Department of Physics and Astronomy, MS-108, P. O. Box 1892, Houston, TX 77251

⁹Istituto Nazionale di Fisica Nucleare, Sezione di Padova, I-35131 Padova, Italy

¹⁰Dipartimento di Fisica “G. Galilei”, Università di Padova, I-35131 Padova, Italy

¹¹Istituto Nazionale di Fisica Nucleare, Sezione di Perugia, I-06123 Perugia, Italy

¹²Dipartimento di Fisica, Università degli Studi di Perugia, I-06123 Perugia, Italy

¹³Santa Cruz Institute for Particle Physics, Department of Physics and Department of Astronomy and Astrophysics, University of California at Santa Cruz, Santa Cruz, CA 95064, USA

¹⁴CNRS, IRAP, F-31028 Toulouse cedex 4, France

¹⁵Université de Toulouse, UPS-OMP, IRAP, Toulouse, France

¹⁶Department of Physics, Center for Cosmology and Astro-Particle Physics, The Ohio State University, Columbus, OH 43210, USA

¹⁷Dipartimento di Fisica “M. Merlin” dell’Università e del Politecnico di Bari, I-70126 Bari, Italy

¹⁸Istituto Nazionale di Fisica Nucleare, Sezione di Bari, 70126 Bari, Italy

¹⁹Laboratoire Leprince-Ringuet, École polytechnique, CNRS/IN2P3, Palaiseau, France

²⁰Institut de Ciències de l’Espai (IEEC-CSIC), Campus UAB, 08193 Barcelona, Spain

²¹INAF-Istituto di Astrofisica Spaziale e Fisica Cosmica, I-20133 Milano, Italy

²²Artep Inc., 2922 Excelsior Springs Court, Ellicott City, MD 21042, resident at Naval Research Laboratory, Washington, DC 20375

²³National Research Council Research Associate, National Academy of Sciences, Washington, DC 20001, resident at Naval Research Laboratory, Washington, DC 20375

²⁴Instituto de Astronomía y Física del Espacio, Parbellón IAFE, Cdad. Universitaria, Buenos Aires,

Argentina

²⁵NASA Goddard Space Flight Center, Greenbelt, MD 20771, USA

²⁶Laboratoire Univers et Particules de Montpellier, Université Montpellier 2, CNRS/IN2P3, Montpellier, France

²⁷Department of Physics, Stockholm University, AlbaNova, SE-106 91 Stockholm, Sweden

²⁸The Oskar Klein Centre for Cosmoparticle Physics, AlbaNova, SE-106 91 Stockholm, Sweden

²⁹Royal Swedish Academy of Sciences Research Fellow, funded by a grant from the K. A. Wallenberg Foundation

³⁰Institut universitaire de France, 75005 Paris, France

³¹Agenzia Spaziale Italiana (ASI) Science Data Center, I-00044 Frascati (Roma), Italy

³²Dipartimento di Fisica, Università di Udine and Istituto Nazionale di Fisica Nucleare, Sezione di Trieste, Gruppo Collegato di Udine, I-33100 Udine, Italy

³³Space Science Division, Naval Research Laboratory, Washington, DC 20375, USA

³⁴Université Bordeaux 1, CNRS/IN2p3, Centre d'Études Nucléaires de Bordeaux Gradignan, 33175 Gradignan, France

³⁵Osservatorio Astronomico di Trieste, Istituto Nazionale di Astrofisica, I-34143 Trieste, Italy

³⁶Department of Physical Sciences, Hiroshima University, Higashi-Hiroshima, Hiroshima 739-8526, Japan

³⁷Department of Physics and Astrophysics, Nagoya University, Chikusa-ku Nagoya 464-8602, Japan

³⁸INAF Istituto di Radioastronomia, 40129 Bologna, Italy

³⁹Institut für Astronomie und Astrophysik, Universität Tübingen, D 72076 Tübingen, Germany

⁴⁰Center for Space Plasma and Aeronomic Research (CSPAR), University of Alabama in Huntsville, Huntsville, AL 35899

⁴¹Department of Physics, Royal Institute of Technology (KTH), AlbaNova, SE-106 91 Stockholm, Sweden

⁴²Science Institute, University of Iceland, IS-107 Reykjavik, Iceland

⁴³Research Institute for Science and Engineering, Waseda University, 3-4-1, Okubo, Shinjuku, Tokyo 169-8555, Japan

⁴⁴Funded by contract ERC-StG-259391 from the European Community

⁴⁵Department of Physics and Department of Astronomy, University of Maryland, College Park, MD 20742

⁴⁶Mullard Space Science Laboratory, University College London, Holmbury St. Mary, Dorking, Surrey, RH5 6NT, UK

⁴⁷Center for Research and Exploration in Space Science and Technology (CRESST) and NASA Goddard Space Flight Center, Greenbelt, MD 20771

⁴⁸Istituto Nazionale di Fisica Nucleare, Sezione di Roma “Tor Vergata”, I-00133 Roma, Italy

ABSTRACT

33

34

We present observations of the young Supernova remnant (SNR) RX J1713.7–3946 with the *Fermi* Large Area Telescope (LAT). We clearly detect a source positionally coincident with the SNR. The source is extended with a best-fit extension of $0.55^\circ \pm 0.04^\circ$ matching the size of the non-thermal X-ray and TeV gamma-ray emission from the remnant. The positional coincidence and the matching extended emission allows us to identify the LAT source with the supernova remnant RX J1713.7–3946. The spectrum of the source can be described by a very hard power-law with a photon index of $\Gamma = 1.5 \pm 0.1$ that coincides in normalization with the steeper H.E.S.S.-detected gamma-ray spectrum at higher

⁴⁹Department of Physics and Astronomy, University of Denver, Denver, CO 80208, USA

⁵⁰Hiroshima Astrophysical Science Center, Hiroshima University, Higashi-Hiroshima, Hiroshima 739-8526, Japan

⁵¹Institute of Space and Astronautical Science, JAXA, 3-1-1 Yoshinodai, Chuo-ku, Sagamihara, Kanagawa 252-5210, Japan

⁵²Max-Planck Institut für extraterrestrische Physik, 85748 Garching, Germany

⁵³Max-Planck-Institut für Physik, D-80805 München, Germany

⁵⁴Institut für Physik und Astronomie, Universität Potsdam, 14476 Potsdam, Germany

⁵⁵Deutsches Elektronen Synchrotron DESY, D-15738 Zeuthen, Germany

⁵⁶Institut für Astro- und Teilchenphysik and Institut für Theoretische Physik, Leopold-Franzens-Universität Innsbruck, A-6020 Innsbruck, Austria

⁵⁷Department of Physics, University of Washington, Seattle, WA 98195-1560, USA

⁵⁸Solar-Terrestrial Environment Laboratory, Nagoya University, Nagoya 464-8601, Japan

⁵⁹Partially supported by the International Doctorate on Astroparticle Physics (IDAPP) program

⁶⁰Institut für Theoretische Physik and Astrophysik, Universität Würzburg, D-97074 Würzburg, Germany

⁶¹Institució Catalana de Recerca i Estudis Avançats (ICREA), Barcelona, Spain

⁶²Consorzio Interuniversitario per la Fisica Spaziale (CIFS), I-10133 Torino, Italy

⁶³INTEGRAL Science Data Centre, CH-1290 Versoix, Switzerland

⁶⁴NASA Postdoctoral Program Fellow, USA

⁶⁵Dipartimento di Fisica, Università di Roma “Tor Vergata”, I-00133 Roma, Italy

⁶⁶Department of Physics and Mathematics, Aoyama Gakuin University, Sagamihara, Kanagawa, 252-5258, Japan

energies. The broadband gamma-ray emission is consistent with a leptonic origin as the dominant mechanism for the gamma-ray emission.

Subject headings: gamma-ray: observations; ISM: supernova remnants, ISM:individuals:RX J1713.7-3946, acceleration of particles, radiation mechanisms: non-thermal

1. Introduction

Gamma-ray observations of shell-type supernova remnants (SNRs) hold great promise to help understanding the acceleration of cosmic rays (CRs). These particles – arriving at Earth mostly in the form of protons – are thought to be accelerated by a mechanism called *diffusive shock* acceleration (Bell 1978; Blandford & Ostriker 1978; Jones & Ellison 1991; Malkov & Drury 2001) in the shocks of supernova explosions up to energies around the “knee” in the spectrum of cosmic rays ($\sim 10^{15}$ eV). In particular, X-ray and TeV gamma-ray observations of young SNRs such as Cas A (Hwang et al. 2004; Gotthelf et al. 2001; Albert et al. 2007; Abdo et al. 2010b), or RX J1713.7–3946 (Koyama et al. 1997; Uchiyama et al. 2002; Aharonian et al. 2006, 2007) have confirmed the existence of relativistic particles in the shock waves. Young SNRs are preferred targets for seeing particle acceleration at work since in these objects the shocks are still strong and actively accelerating particles to the highest energies. Gamma-ray instruments have the angular resolution to spatially resolve some of the closer SNRs.

RX J1713.7–3946 (also known as G347.3–0.5) is a young “historical” remnant suggested to be associated with the appearance of a guest star in the constellation of Scorpius in AD393 by Wang et al. (1997). RX J1713.7–3946 is located in the Galactic plane (at $l = 347.3^\circ$, $b = -0.5^\circ$) and was discovered in soft X-rays in 1996 in the ROSAT all-sky survey (Pfeffermann & Aschenbach 1996). At a suggested distance of 1 kpc (Koyama et al. 1997; Fukui et al. 2003; Cassam-Chenaï et al. 2004) with angular diameter $\sim 65' \times 55'$, the size of the shell is ~ 20 pc. Its properties are strikingly dominated by non-thermal activity. Its X-ray emission shows a featureless spectrum interpreted to be completely dominated by X-ray synchrotron emission from ultra-relativistic electrons (Koyama et al. 1997; Slane et al. 1999; Tanaka et al. 2008). The thermal X-ray emission as well as the radio emission are extremely faint (Lazendic et al. 2004). Detailed X-ray observations with *Chandra* and *XMM-Newton* unveiled a complex structure of filaments and knots in the shell of the SNR – in particular in the western part (Uchiyama et al. 2003; Lazendic et al. 2004; Cassam-Chenaï et al. 2004; Acero et al. 2009). A recent study with the *Suzaku* satellite extended the X-ray spectrum to ~ 40 keV, a measurement that enabled the determination of the parent electron spectrum in the energy range where the spectrum cuts off (Tanaka et al. 2008).

67 RX J1713.7–3946 is the first SNR for which TeV gamma-ray emission was clearly de-
 68 tected emerging from the shell. H.E.S.S. measurements provided the first-ever resolved
 69 gamma-ray emission at TeV energies. The TeV emission closely matches the non-thermal
 70 X-ray emission as demonstrated by Aharonian et al. (2006). The energy spectrum of
 71 RX J1713.7–3946 has been measured up to ~ 100 TeV, clearly demonstrating particle
 72 acceleration to beyond these energies in the shell of the SNR.

73 While the non-thermal X-rays detected in the shells of young SNRs are clearly generated
 74 through synchrotron emission by ultra-relativistic electrons (Koyama et al. 1997), the picture
 75 of the particle population radiating the gamma rays is not so clear. The main argument
 76 revolves around two main emission mechanisms (Aharonian et al. 2006; Katz & Waxman
 77 2008; Berezhko & Völk 2008; Porter et al. 2006; Ellison & Vladimirov 2008; Morlino et al.
 78 2009), but so far, conclusive evidence for either possibility is still missing. One scenario
 79 suggests a connection of the TeV gamma-ray emission with accelerated protons (CRs) by
 80 invoking the interaction of these protons with interstellar material generating neutral pions
 81 (π^0 s) which in turn decay into gamma rays. A second competing channel exists in the
 82 inverse Compton scattering of the photon fields in the surroundings of the SNR by the same
 83 relativistic electrons that generate the synchrotron X-ray emission. This channel naturally
 84 accounts for the close resemblance between the X-ray and the TeV gamma-ray images.
 85 Several ways have been suggested to distinguish between these two scenarios (see e.g. Morlino
 86 et al. 2009) but one of the most promising seems to be the broadband modeling of the spectral
 87 energy distribution (SED). In this regard, observations of young SNRs with the LAT on
 88 board the *Fermi* Gamma-Ray Space Telescope (*Fermi*) are of particular importance since
 89 the LAT detects gamma rays in the energy range that bridges sensitive measurements with
 90 X-ray satellites such as *Chandra* and *XMM-Newton* and TeV gamma-ray telescopes such as
 91 H.E.S.S., VERITAS or MAGIC.

92 2. Observation and Analysis

93 The *Fermi*-LAT is a pair-conversion gamma-ray telescope with a precision tracker and
 94 calorimeter, each consisting of a 4×4 array of 16 modules, a segmented anti-coincidence
 95 detector (ACD) that covers the tracker array, and a programmable trigger and data ac-
 96 quisition system. The incoming gamma rays produce electron-positron pairs in the tracker
 97 subsystem, which allow a reconstruction of the directions of the primary gamma rays using
 98 the information provided by the 36 layers of silicon strip detectors in the tracker. The energy
 99 of the incoming gamma ray is determined from the energy deposited by the electromagnetic
 100 showers in the segmented CsI calorimeter. The ACD subsystem is used as a veto against

101 the great majority of cosmic rays that trigger the LAT. The energy range of the LAT is 20
102 MeV to > 300 GeV with an angular resolution for events converting in the front part of the
103 detector of approximately 3.5° at 100 MeV, improving to about 0.1° at 10 GeV (defined as
104 the 68% containment radius of the LAT point-spread function or PSF). Full details on the
105 instrument and the on-board and ground data processing are given in (Atwood et al. 2009).

106 The LAT normally operates in a scanning mode (the “sky survey” mode) that covers
107 the whole sky every two orbits (~ 3 h). We use data taken in this mode from the commence-
108 ment of scientific operations on 2008 August 4 to 2010 August 4. The data were prepared
109 and analyzed using the LAT Science Tools package (v9r16p1), which is available from the
110 *Fermi* Science Support Center ¹. Only events satisfying the standard low-background event
111 selection (the so-called “Diffuse” class events) and coming from zenith angles $< 105^\circ$ (to
112 greatly reduce the contribution by Earth albedo gamma rays, see Abdo et al. 2009a) were
113 used in the present analysis. We use all gamma rays with energy > 500 MeV within a
114 $20^\circ \times 20^\circ$ region of interest (ROI) centered at the nominal position of RX J1713.7–3946
115 ($\alpha = 258.39^\circ$, $\delta = 39.76^\circ$). We chose a lower bound of 500 MeV for this analysis for two
116 reasons: Due to the relative hardness of the spectrum of RX J1713.7–3946 compared to
117 the Galactic diffuse background, photons with energies below 500 MeV are not effective in
118 constraining morphology or spectral shape of the source. Additionally, the broadening of
119 the PSF at low energies might lead to systematic problems of confusion with neighboring
120 sources in this densely populated region of the sky. To further reduce the effect of Earth
121 albedo backgrounds, any time intervals when the Earth was appreciably in the field of view
122 (specifically, when the center of the field of view was more than 52° from the zenith) as well
123 as any time intervals when parts of the ROI were observed at zenith angles $> 105^\circ$ were also
124 excluded from the analysis. The spectral analysis was performed based on the P6v3 version
125 of post-launch instrument response functions (IRFs) which take into account pile-up and
126 accidental coincidence effects in the detector subsystems (Rando et al. 2009). The binned
127 maximum-likelihood mode of *gtlike*, which is part of the ScienceTools, was used to determine
128 the intensities and spectral parameters presented in this paper.

¹<http://fermi.gsfc.nasa.gov/ssc/>

2.1. Background sources

129

130 We adopt a background model for the region which includes components describing
 131 the diffuse Galactic and isotropic gamma-ray emission ². It also includes all point sources
 132 within our ROI which are identified in the 1FGL catalog (Abdo et al. 2010a) except 1FGL
 133 1711.7–3944c which is spatially coincident with RX J1713.7–3946. All 1FGL sources are
 134 modeled with a power-law spectrum using the flux and spectral index values obtained from
 135 the catalog. Exceptions are the known pulsars in the ROI which we model with a power-law
 136 with exponential cutoff spectral model. As the parameters for this spectral model cannot
 137 be obtained from the 1FGL catalog, we keep the flux, spectral index and cutoff energy of
 138 the known pulsars as free parameters in the maximum likelihood fits of the ROI. Figure 1
 139 shows two maps of the point-source detection significance, evaluated at each point in the map
 140 (TS map) for the region around RX J1713.7–3946 using photons with energies > 500 MeV.
 141 The flux of the source is not permitted to be negative, this is why negative fluctuations are
 142 not visible. The detection significance is shown in terms of the test statistic (TS) of the
 143 likelihood fit. The TS value is defined as $TS=2(\ln L_1/L_0)$, proportional to the logarithm
 144 of the likelihood ratio between a point-source hypothesis (L_1) and the null hypothesis of
 145 pure background (L_0) (Mattox et al. 1996). The significance contours of the TeV emission
 146 observed from the SNR by the H.E.S.S. telescope array (Aharonian et al. 2006) are overlaid
 147 on the maps. Panel (a) shows the TS map characterizing the excess emission found in the
 148 region around RX J1713.7–3946 over our background model described above. A significant
 149 TS value is found within the spatial extent of the SNR but also in several regions outside of
 150 its shell.

151 We identify three regions of excess gamma-ray emission which are likely not associated
 152 with the SNR but belong to background sources not recognized in the first *Fermi* catalog
 153 (1FGL). Due to the longer integration time of our analysis (24 months vs. 11 months in the
 154 catalog) and the corresponding improved sensitivity, the appearance of additional sources
 155 in our region of interest is expected. We simply denote these sources with the identifier *A*,
 156 *B*, *C*. The source positions are shown in Figure 1 and given in Table 2. The location of
 157 source *A* is consistent with a weak radio source (Lazendic et al. 2004). It is further identified
 158 in an internal update of the *Fermi* LAT catalog using 24 months of data. Source *B* is
 159 only 11' from the catalog source 1FGL J1714.5–3830c and could be an artifact caused by
 160 unmodeled emission from 1FGL J1714.5–3830c if this source were spatially extended as has
 161 been tentatively suggested by Castro & Slane (2010). 1FGL J1714.5–3830c is modeled as a

²The LAT standard diffuse emission models (*gll_iem_v02.fits* and *isotropic_iem_v02.fits*), available at <http://fermi.gsfc.nasa.gov/ssc/data/access/lat/BackgroundModels.html>

162 point source in the 1FGL catalog. However, the catalog source is spatially coincident with
 163 the SNR CTB 37A which has an extent in radio of $\sim 15'$ (Green 2004). A detailed study of
 164 the morphology of this source is in progress but beyond the scope of this publication as the
 165 exact morphology of the CTB 37A source does not significantly affect the spectral analysis
 166 of RX J1713.7–3946. For simplicity we just assume the emission from this region to be
 167 described by two independent point sources, 1FGL J1714.5–3830c and source *B*. The third
 168 additional background source *C* shown in Figure 1 may be associated with RX J1713.7–3946.
 169 It is very close to RX J1713.7–3946, located about $35'$ from the center of the SNR. However,
 170 it is spatially consistent with a local enhancement of molecular gas, observed via the radio
 171 emission from the CO ($J=1\rightarrow 0$) transition (Dame et al. 2001). Furthermore, we will show
 172 below (see Table 2) that in a combined likelihood analysis of the spectra of RX J1713.7–3946
 173 and the surrounding background sources the emission from source *C* is considerably softer
 174 than the gamma-ray emission from the SNR. In fact, both the spectral index and the intensity
 175 of the source are consistent with expectations of gamma-ray emission from a small cloud of
 176 molecular gas. Nevertheless, we cannot reject the possibility that at least part of the emission
 177 attributed to the additional background source *C* is originating from the SNR shell. While
 178 we consider source *C* an independent point source in our standard background model of the
 179 ROI, we repeat the spectral analysis with a model without this source and account for the
 180 difference in our estimation of systematic uncertainties. Panel (b) in Figure 1 shows the
 181 detection significance map for the region around RX J1713.7–3946 ($E > 500$ MeV) with
 182 our standard background model accounted for. A comparison with the significance contours
 183 from H.E.S.S. suggests a spatially extended emission from the shell of the SNR rather than
 184 a single point source.

185 2.2. Centroid and Angular Extent

186 We study the morphology of the emission associated with RX J1713.7–3946 with a
 187 series of maximum likelihood fits, comparing the TS value for different hypotheses about the
 188 shape and extent of the source. We fitted the extension (and position) of the gamma-ray
 189 emission with a disk of varying radius. The emission is found to be significantly extended;
 190 the best-fit position (RA, Dec = $258.50^\circ \pm 0.04^\circ_{\text{stat}}$, $-39.91^\circ \pm 0.05^\circ_{\text{stat}}$) is consistent with the
 191 center of the SNR within 0.2° and the best-fit radius is $0.55^\circ \pm 0.04^\circ$. This size is consistent
 192 with that of the X-ray SNR given in Green (2004) as $1.1^\circ \times 0.9^\circ$ in diameter. To confirm
 193 these fits, we test a single point source at the location of the highest excess in the TS map
 194 within the shell of the SNR. We further test a spatially extended source defined by the
 195 shape of the H.E.S.S. significance contours of RX J1713.7–3946 and an extended source
 196 as a uniform disk of 0.55° radius. Finally, we consider two and three independent point

197 sources within the shell of the SNR located at the most prominent peaks in the TS map.
 198 A power-law spectrum with integrated flux (between 1 and 300 GeV) and spectral index as
 199 free parameters is assumed for each of the hypotheses. The detailed setup of the likelihood
 200 fit is identical to the one used for the spectral analysis and described with that analysis
 201 (Section 2.3). Table 1 shows the flux, and spectral index of the tested shape and its TS
 202 value in comparison to the background model. The TS values are suggestive of extended
 203 gamma-ray emission from RX J1713.7–3946. The H.E.S.S. significance map as well as the
 204 uniform disk have a difference in TS of $\Delta TS = 61$ or 58 (H.E.S.S./Disk) relative to a single
 205 point source and a $\Delta TS = 43$ or 40 (H.E.S.S./Disk) relative to a set of 3 point sources within
 206 the shell of RX J1713.7–3946. However, the TS value in a comparison to the background
 207 model for both the H.E.S.S. significance map ($TS = 77$) and the uniform disk ($TS = 79$)
 208 are almost identical, demonstrating that we are not sensitive to the detailed shape of the
 209 emission region. For the models of RX J1713.7–3946 considered, the TS value is expected
 210 to follow a χ^2 -distribution with two degrees of freedom in the case that no source is present
 211 (Mattox et al. 1996) and therefore can be converted to a detection significance of $\sim 8.5\sigma$ for
 212 both the H.E.S.S. template and the uniform disk model. The positional and the angular-size
 213 coincidence with the X-ray and TeV gamma-ray emission strongly favors an identification of
 214 the LAT source with the SNR RX J1713.7–3946.

215 Fig. 2 shows a series of LAT gamma-ray counts maps of the sky surrounding RX J1713.7–3946.
 216 We choose an energy threshold of 3 GeV for these maps, higher than the analysis threshold
 217 of 500 MeV, to enhance their resolution. The counts maps are smoothed with an 0.3° wide
 218 Gaussian kernel. This width corresponds to the size of the LAT PSF at 3 GeV (the 39%
 219 containment radius of a 2-D gaussian), averaged over front and back conversions and over all
 220 incident angles. Locations of 1FGL catalog sources in the region are marked by squares. Our
 221 additional background sources are denoted by circles and labeled. The black lines again dis-
 222 play the contours of the H.E.S.S. significance map of RX J1713.7–3946. Panel (a) shows all
 223 counts in the region. The emission coinciding with RX J1713.7–3946 is faint; the counts map
 224 is dominated by the Galactic diffuse emission as well as emission from 1FGL J1714.5–3830c
 225 and 1FGL J1705.5–4034c. Panel (b) shows a residual counts map after subtraction of our
 226 background model. On this panel a clear excess within the shell of RX J1713.7–3946 is vis-
 227 ible. Panel (c) finally shows the residual counts after subtraction of our background model
 228 as well as the emission from RX J1713.7–3946 (using the H.E.S.S. significance map as the
 229 template for the spatial extension). The residual counts are consistent with the expected
 230 statistical fluctuations, i.e the region around the SNR is well described by our model.

2.3. Spectral Analysis

231

232 We adopt the spatial extension model based on the H.E.S.S. significance map as the
 233 default model for the analysis of the spectrum of RX J1713.7–3946. As discussed in the
 234 previous section, the LAT is not able to distinguish between the two extended source models
 235 that we tested. Therefore, we compare the obtained spectrum from the default model to the
 236 results derived from a uniform disk source model and include the difference in the systematic
 237 uncertainty of the spectrum. In the first step of the spectral analysis we perform a maximum
 238 likelihood fit of the spectrum of RX J1713.7–3946 in the energy range between 500 MeV
 239 and 400 GeV using a power-law spectral model with integral flux and spectral index as free
 240 parameters. To accurately account for correlations between close-by sources we also allow
 241 the integral fluxes and spectral indices of the nearby 1FGL and sources A , B , C ($< 3^\circ$ from
 242 the center of the ROI) to be free for the likelihood maximization, as well as the spectral
 243 parameters of identified LAT pulsars, instead of fixing them to the 1FGL catalog values. We
 244 redetermine in our fit the normalization of the Galactic diffuse emission model, the index of
 245 an energy dependent (power-law) multiplicative correction factor to it, and the normalization
 246 of the isotropic component. This accounts for localized variations in the spectrum of the
 247 diffuse emission in the fit which are not considered in the global model.

248 For the Galactic diffuse emission, we find a normalization factor of 0.93 ± 0.01 in our
 249 region of interest and a spectral correction factor index of 0.019 ± 0.002 (the positive sign
 250 corresponds to a spectrum that is harder than in the model). The normalization factor for
 251 the isotropic component is 1.17 ± 0.05 . These factors demonstrate the good agreement of
 252 the local brightness and spectrum of the diffuse gamma-ray emission with the global diffuse
 253 emission model. Table 2 summarizes the source parameters obtained as results from this
 254 fit. The table includes the spectral parameters and the TS values of all fitted sources. The
 255 flux above 1 GeV obtained for RX J1713.7–3946 with our default background model is
 256 $F_{1000} = (2.8 \pm 0.7) \times 10^{-9} \text{ cm}^{-2} \text{ s}^{-1}$ and the spectral index is $\Gamma = 1.50 \pm 0.11$. Figure 3
 257 shows the uncertainty band obtained from this fit.

258 In a second step we perform a maximum likelihood fit of the flux of RX J1713.7–3946
 259 in 7 independent logarithmically spaced energy bands from 500 MeV to 400 GeV (using the
 260 spectral model and parameters obtained in the previous fit) to obtain a spectral energy dis-
 261 tribution (SED) for the SNR. The resulting SED is displayed in Figure 3 as black error bars.
 262 We require a test statistic value of $\text{TS} \geq 4$ in each band to draw a data point corresponding
 263 to a 2σ detection significance. This criterion is not fulfilled for the lowest two energy bands
 264 500 MeV–1.3 GeV and 1.3 GeV–3.4 GeV and accordingly we show 95% flux upper limits for
 265 these bands.

266 In a final step we estimate the systematic uncertainty on the obtained spectral parame-

267 ters by repeating the maximum likelihood analysis for several variations of our default model.
 268 Specifically, we varied the source shape template, the background sources, and the model
 269 of the Galactic diffuse emission. The spectral analysis was performed: a) with the uniform
 270 disk shape replacing the H.E.S.S. significance map template; b) with the closest background
 271 source C removed from the model (see also discussion above); c) using a preliminary list of
 272 sources from the 2FGL catalog in development within the LAT collaboration; d) replacing
 273 the standard diffuse emission model by a refined model that is currently being evaluated in
 274 the collaboration for source analysis for the 2FGL catalog (refined with 24 months of data
 275 and with finer gas maps); e) replacing the standard diffuse model by a model based on the
 276 GALPROP code ³ used in the *Fermi* LAT analysis of the isotropic diffuse emission. The
 277 GALPROP model is described in Abdo et al. (2010c). For e), i.e. the GALPROP-based
 278 model, we considered the various components of the diffuse emission model separately for
 279 which we then individually fit the normalizations in our likelihood analysis. The compo-
 280 nents are gamma rays produced by inverse Compton emission, gamma rays produced by
 281 interactions of CRs with atomic and ionized interstellar gas and gamma rays produced in
 282 the interactions of CRs with molecular gas. The model component describing the gamma
 283 ray intensity from interactions with molecular gas is further subdivided into seven ranges of
 284 Galactocentric distance to accommodate localized variations of the CR and molecular gas
 285 density along the line of sight which are not accounted for in the model.

286 The same model of the isotropic component was used for all model variations a)–
 287 e). From the model variations a) – e) we obtain a systematic uncertainty of +0.08/-
 288 0.10 for the spectral index of RX J1713.7–3946 and a systematic uncertainty of (+0.6/-
 289 0.7) $\times 10^{-9}$ cm⁻² s⁻¹ for the flux above 1 GeV on top of the statistical uncertainty. The
 290 systematic uncertainty of the derived flux and spectral index related to the uncertainty in
 291 the LAT effective area was evaluated separately. The uncertainty of the LAT effective area –
 292 estimated from observations of Vela (Abdo et al. 2009b) and the Earth Albedo (Abdo et al.
 293 2009a) – ranges from 10% at 500 MeV to 20% at ≥ 10 GeV. The impact on the spectral pa-
 294 rameters of RX J1713.7–3946 is a systematic uncertainty of ± 0.05 for the spectral index and
 295 a systematic uncertainty of ± 0.4 for the flux above 1 GeV. The gray band in Figure 3 displays
 296 the superposition of all uncertainty bands obtained in our variations of the default model.
 297 Figure 4 depicts the model variation (b) resulting in the softest spectrum together with the
 298 fluxes in individual energy bands (black error bars) derived for model (b) using the same
 299 procedure as for the default model described above. The range of systematic uncertainty is
 300 particularly important to consider for comparisons of the spectrum to pion-decay dominated

³GALPROP is a software package for calculating the diffuse Galactic gamma-ray emission based on a model of cosmic-ray propagation in the Galaxy. See <http://galprop.stanford.edu/> for details and references

301 gamma-ray emission models which are generally expected to be softer than inverse Compton
 302 dominated gamma-ray emission models.

303 3. Discussion

304 The positional coincidence between the extended gamma-ray emission detected by the
 305 *Fermi*-LAT at the position of RX J1713.7–3946 strongly suggests a physical association be-
 306 tween the GeV gamma-ray emission and this young SNR. In addition, the region of bright-
 307 est LAT gamma-ray emission coincides with the northwestern part of the SNR. From CO
 308 ($J = 1 - 0$) observations Fukui et al. (2003) and Moriguchi et al. (2005) suggested that this
 309 part of the SNR is undergoing complex interactions between the supernova shock wave and
 310 a molecular cloud. This part is also the brightest region in non-thermal X-rays and in TeV
 311 gamma rays. The match between the locations of brightest emission suggests that the GeV
 312 emission is also generated by the population of relativistic particles responsible for the TeV
 313 gamma-ray and non-thermal X-ray emission.

314 The origin of the TeV gamma-ray emission from RX J1713.7–3946 has been a matter
 315 of active debate (see Zirakashvili & Aharonian 2010, and references therein). There are two
 316 competing processes potentially responsible for the shell-like TeV gamma-ray emission from
 317 RX J1713.7–3946: Inverse Compton (IC) scattering on the cosmic microwave background
 318 by relativistic electrons (leptonic model) and π^0 -decay gamma rays resulting mainly from
 319 inelastic collisions between relativistic protons and ambient gas nuclei (hadronic model). It is
 320 generally accepted that diffusive shock acceleration (DSA) operates at supernova shocks pro-
 321 ducing high-energy protons and electrons. However, injection mechanisms of supra-thermal
 322 particles are poorly known so that the current theory cannot tell us about the number of
 323 relativistic protons and electrons produced at shocks. This makes it difficult to reliably
 324 predict the levels of leptonic and hadronic gamma-rays.

325 The lack of thermal X-ray lines provided a stringent constraint on the gamma-ray pro-
 326 duction mechanisms. The luminosity of hadronic gamma-rays scales as $\bar{n}_H W_p$, where \bar{n}_H
 327 denotes the gas density averaged over the emission volume (where accelerated protons are
 328 assumed to be uniformly distributed), $W_p = \xi E_{\text{SN}}$ is a total energy content of accelerated
 329 protons, and $E_{\text{SN}} \sim 10^{51}$ erg is the total kinetic energy released by the SN explosion. The
 330 lack of thermal X-ray emission in SNR RX J1713.7–3946 (Slane et al. 1999; Tanaka et al.
 331 2008) severely restricts the gas density in the SNR to be small. Ellison et al. (2010) have
 332 performed calculations of thermal X-ray emission from shocked plasma with non-equilibrium
 333 ionization in the case of uniform ambient density, following a hydrodynamic evolution with
 334 which non-linear DSA theory is coupled; they found that the shocked gas densities required

335 for consistency with the hadronic model are $n_{\text{H}} \lesssim 0.2 \text{ cm}^{-3}$. It should be noted that, taking
 336 $E_{\text{SN}} = 2 \times 10^{51} \text{ erg}$, one needs $\xi \sim 1$ (i.e., extremely efficient acceleration) for $\bar{n}_{\text{H}} = 0.1 \text{ cm}^{-3}$
 337 and $d = 1 \text{ kpc}$. The extremely efficient (more efficient than usually assumed) transformation
 338 of the supernova kinetic energy into accelerated particles may lead to very low shocked gas
 339 temperature (Drury et al. 2009), which in turn could change the density requirement.

340 The measurements of GeV gamma-ray emission obtained with the *Fermi*-LAT pre-
 341 sented in this paper provide new, crucial information about the particle population respon-
 342 sible for the gamma-ray emission. We have measured the gamma-ray spectrum of SNR
 343 RX J1713.7–3946 in the energy range from 500 MeV to 400 GeV and found that the spectrum
 344 can be characterized by a hard power law with photon index $\Gamma = 1.5 \pm 0.1(\text{stat}) \pm 0.1(\text{sys})$,
 345 smoothly connecting with the steeper TeV gamma-ray spectrum measured with H.E.S.S.
 346 Note that the measured gamma-ray spectrum of RX J1713.7–3946 now covers five orders of
 347 magnitude in energy, unprecedented for SNRs.

348 The hard power-law shape in the *Fermi*-LAT energy range with photon index of $\Gamma =$
 349 1.5 ± 0.1 qualitatively agrees with the expected IC spectrum of the leptonic model, as il-
 350 lustrated in both Figures 3 and 4. If the leptonic model explains the gamma-ray spectrum,
 351 the *Fermi*-LAT spectrum is emitted by a power-law part of the accelerated electrons, and
 352 therefore we can deduce the power-law index of electrons from the measured photon index.
 353 Using $\Gamma = 1.5 \pm 0.1$, we obtain $s_e = 2\Gamma - 1 = 2.0 \pm 0.2$. The energy flux ratio of the
 354 observed synchrotron X-ray emission and the gamma-ray emission means that the average
 355 magnetic field is weak, $B \simeq 10 \mu\text{G}$ (Aharonian et al. 2006; Porter et al. 2006; Ellison et al.
 356 2010). The maximum energy of electrons is then $E_{e,\text{max}} \sim 20\text{--}40 \text{ TeV}$ as determined from
 357 the *Suzaku* X-ray spectrum (Tanaka et al. 2008). The presence of synchrotron X-ray fila-
 358 ments varying on yearly timescales (Uchiyama et al. 2007), if interpreted as being due to fast
 359 electron acceleration and synchrotron cooling, requires $B \sim 0.1\text{--}1 \text{ mG}$, which is difficult to
 360 reconcile with the weak average field. Alternatively, the X-ray variability may be caused by
 361 time-variable turbulent magnetic fields (Bykov et al. 2008) which require a smaller magnetic
 362 field strength. The filamentary structures and variability in X-rays should be attributed to
 363 locally enhanced magnetic fields in the case of the leptonic model (Pohl et al. 2005).

364 As shown in Fig. 3, several groups have previously presented calculations of IC gamma-
 365 ray spectra. Detailed comparisons between the observed total GeV–TeV spectrum and IC
 366 models show that none of the previous IC models matches exactly with the data. Some
 367 additional complications would need to be introduced to realize a better description of the
 368 gamma-ray data. For example, the shape of the total IC spectrum could be modified if we
 369 add a second population of electrons (or even multiple populations) which has a different
 370 maximum energy (see Tanaka et al. 2008; Yamazaki et al. 2009). Yet another way of modi-

371 fying the IC spectral shape is by invoking more-intense interstellar radiation fields, though
 372 this would require substantial increase in the photon density (see Tanaka et al. 2008).

373 Even in the case of the leptonic model, it is important to constrain the level of π^0 -decay
 374 emission at GeV energies by allowing for a hybrid (leptonic and hadronic) model of the
 375 GeV–TeV gamma-ray spectrum. For proton number index $s = 2$ (assumed to be same as
 376 the electron number index: see e.g. Baring et al. (1999) for a discussion of why relativistic
 377 electron and ion indices should be very similar in non-linear shocks), the GeV flux upper
 378 limit at 1 GeV corresponds to $W_p < 0.3 \times 10^{51} (\bar{n}_H/0.1 \text{ cm}^{-3})^{-1} \text{ erg}$ for $d = 1 \text{ kpc}$, where
 379 \bar{n}_H denotes the hydrogen number density of X-ray/gamma-ray emitting gas. Therefore, the
 380 leptonic model does not necessarily mean the proton content in this SNR is unexpectedly
 381 small.

382 The GeV measurements with *Fermi*-LAT do not agree with the expected fluxes around
 383 1 GeV in most hadronic models published so far (e.g., Berezhko & Völk 2010). Given the
 384 current models of diffusive shock acceleration, we can discard the hadronic origin of the GeV–
 385 TeV gamma-ray emission. The proton number index $s \sim 1.5$ inferred by the LAT spectrum
 386 is as small as the asymptotic index of $s = 1.5$ predicted by extremely efficient CR acceler-
 387 ation (Malkov 1999, see also Ellison & Eichler (1984) for early indications of this limiting
 388 behavior). Unless this asymptotic index is realized in the shock waves of RX J1713.7–3946,
 389 the hard *Fermi*-LAT spectrum cannot be ascribed to the π^0 -decay emission. However, such
 390 a proton energy distribution is not observed in the current models of efficient DSA (Ellison
 391 et al. 2010).

392 4. Summary

393 We have measured the GeV gamma-ray emission from RX J1713.7–3946 with the
 394 *Fermi*-LAT. The emission is extended and shows a size that matches the TeV-detected
 395 gamma-ray emission from this SNR. The gamma-ray spectrum for the SNR has been mea-
 396 sured over more than 5 orders of magnitude combining *Fermi*-LAT and H.E.S.S. observa-
 397 tions. The spectral index in the *Fermi*-LAT band is very hard with a photon index of 1.5 ± 0.1
 398 which is well in agreement with emission scenarios in which the dominant source of emission
 399 is Inverse Compton scattering of ambient photon fields of relativistic electrons accelerated in
 400 the shock front. The dominance of leptonic processes in explaining the gamma-ray emission
 401 does not mean that no protons are accelerated in this SNR, but that the ambient density is
 402 too low to produce a significant hadronic gamma-ray signal. RX J1713.7–3946 is the first
 403 remnant where the combination with H.E.S.S. data yields spectroscopic measurements over
 404 more than 5 decade in energy that, in contrast to many of the other LAT-detected remnants

405 strongly suggests a leptonic origin of the gamma-ray emission.

406 The *Fermi* LAT Collaboration acknowledges generous ongoing support from a number
 407 of agencies and institutes that have supported both the development and the operation of the
 408 LAT as well as scientific data analysis. These include the National Aeronautics and Space
 409 Administration and the Department of Energy in the United States, the Commissariat à
 410 l’Energie Atomique and the Centre National de la Recherche Scientifique / Institut National
 411 de Physique Nucléaire et de Physique des Particules in France, the Agenzia Spaziale Italiana
 412 and the Istituto Nazionale di Fisica Nucleare in Italy, the Ministry of Education, Culture,
 413 Sports, Science and Technology (MEXT), High Energy Accelerator Research Organization
 414 (KEK) and Japan Aerospace Exploration Agency (JAXA) in Japan, and the K. A. Wallen-
 415 berg Foundation, the Swedish Research Council and the Swedish National Space Board in
 416 Sweden.

417 Additional support for science analysis during the operations phase is gratefully acknowl-
 418 edged from the Istituto Nazionale di Astrofisica in Italy and the Centre National d’Études
 419 Spatiales in France.

| Source morphology | Flux ^a | Photon index | TS ^b | R. A. 2000 | Dec. |
|---|-------------------|--------------|-----------------|------------|---------|
| Point source | 1.2 ± 0.7 | 1.85 ± 0.31 | 18 | 257.94° | −39.75° |
| 2 point sources | 0.5 ± 0.5 | 1.68 ± 0.41 | | 257.93° | −39.61° |
| | 1.2 ± 0.9 | 2.13 ± 0.41 | 20 | 257.85° | −39.86° |
| 3 point sources | 0.5 ± 0.5 | 1.69 ± 0.41 | | 257.93° | −39.61° |
| | 1.2 ± 0.2 | 2.10 ± 0.28 | | 257.85° | −39.86° |
| | 0.4 ± 0.3 | 1.61 ± 0.31 | 32 | 259.00° | −39.81° |
| Extended source (H.E.S.S.) ^c | 2.8 ± 0.7 | 1.50 ± 0.11 | 77 | | |
| Extended source (uniform disk) ^d | 3.2 ± 0.7 | 1.49 ± 0.10 | 79 | 258.50° | −39.91° |

^aE>1 GeV, in 10^{−9} cm^{−2} s^{−1}

^bTS value in comparison to a model with no source at the position of RX J1713.7–3946.

^cH.E.S.S. significance map is used as a template for the intensity of the gamma-ray emission.

^dA uniform disk with 0.55° radius is used as a template for the intensity of the gamma-ray emission. The specified coordinates correspond to the center of the disk. These parameters are the best-fit parameters when simultaneously fitting the position and the extension.

Table 1: Results of the morphological analysis of the gamma-ray emission from RX J1713.7–3946. The integral flux between 1 and 300 GeV and the spectral index are the free parameters of the fit and are fitted in the energy range 500 MeV to 400 GeV.

| Source name | Flux ^a | Photon index | Exp. cutoff ^b | TS ^c | R. A. 2000 | Dec. |
|--------------------|-------------------|-----------------|--------------------------|-----------------|------------|---------|
| 1FGL J1705.5–4034c | 2.1 ± 0.7 | 2.16 ± 0.19 | | 20 | | |
| 1FGL J1709.7–4429 | 175 ± 6.4 | 1.74 ± 0.03 | 4.46 ± 0.23 | 50064 | | |
| 1FGL J1714.5–3830c | 9.8 ± 1.3 | 2.47 ± 0.09 | | 228 | | |
| 1FGL J1716.9–3830c | 1.9 ± 1.1 | 2.47 ± 0.34 | | 14 | | |
| 1FGL J1717.9–3729c | 4.9 ± 0.7 | 2.34 ± 0.11 | | 81 | | |
| 1FGL J1718.2–3825 | 8.4 ± 4.3 | 1.64 ± 0.41 | 1.72 ± 0.65 | 165 | | |
| source <i>A</i> | 1.6 ± 0.5 | 2.03 ± 0.17 | | 28 | 258.84° | –40.46° |
| source <i>B</i> | 4.2 ± 1.2 | 2.48 ± 0.16 | | 43 | 258.71° | –38.70° |
| source <i>C</i> | 2.5 ± 0.7 | 2.45 ± 0.22 | | 21 | 257.47° | –39.75° |
| RX J1713.7–3946 | 2.8 ± 0.7 | 1.50 ± 0.11 | | 77 | | |

^aE>1 GeV, in $10^{-9} \text{ cm}^{-2} \text{ s}^{-1}$

^bin GeV

^cDifference in TS value in comparison to a model with no source at the position of the respective source.

Table 2: Results of the spectral analysis of the gamma-ray emission in the ROI centered at RX J1713.7–3946. The integral flux between 1 and 300 GeV and the spectral index are the free parameters of the fit and are fitted in the energy range 500 MeV to 400 GeV.

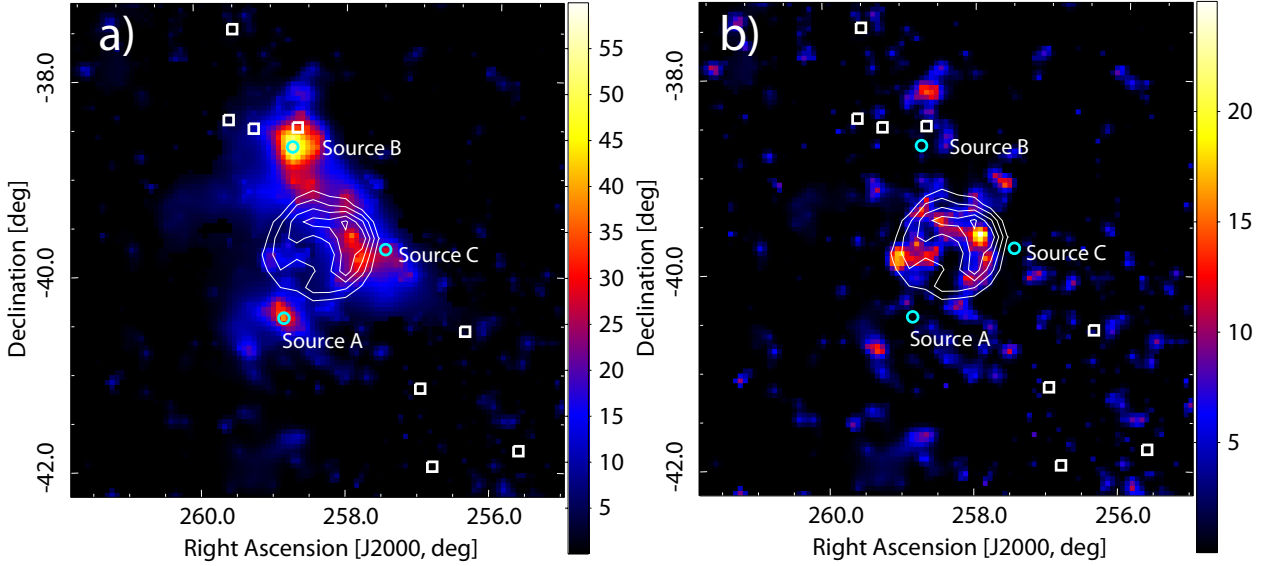


Fig. 1.— **Panel (a):** Map of the test statistic (TS) for a point source in the region around RX J1713.7–3946 obtained in a maximum likelihood fit accounting for the background diffuse emission and 1FGL catalog sources. Only events above 500 MeV have been used in this analysis. H.E.S.S. TeV emission contours are shown in white (Aharonian et al. 2007). Rectangles indicate the positions of 1FGL sources in our background model, Several TS peaks outside the SNR shell are visible. The 3 peaks marked by circles are added as additional sources to our background model (see text). **Panel (b):** Same map as panel (a), but with the 3 additional sources now considered in the background model.

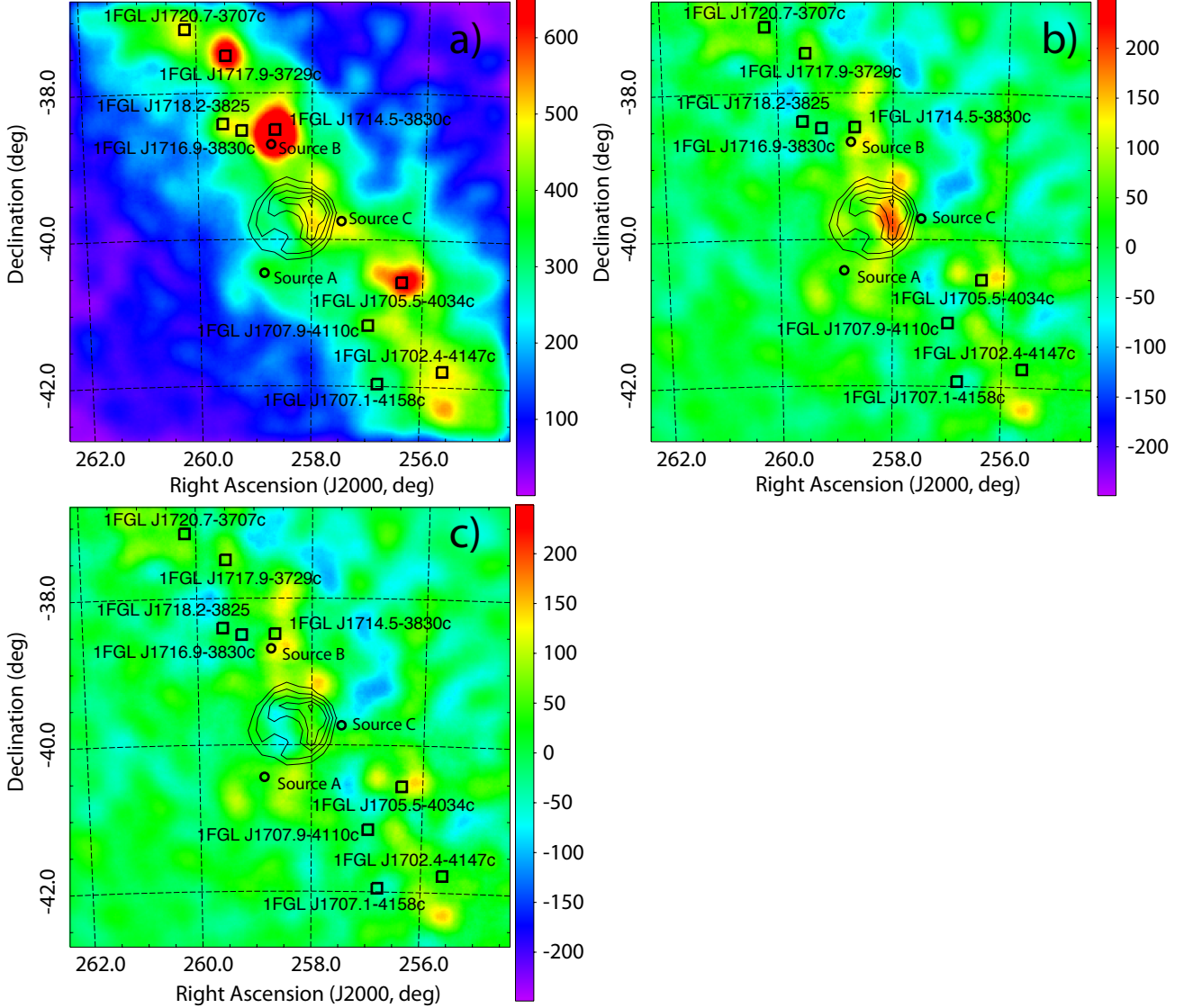


Fig. 2.— **Panel (a):** Counts/sq. deg. observed by the *Fermi* LAT above 3 GeV in the region around RX J1713.7–3946. The map is smoothed with a 0.3° -wide Gaussian kernel corresponding to the width of the LAT PSF at 3 GeV. H.E.S.S. TeV emission contours are shown in black (Aharonian et al. 2007). Rectangles indicate the positions of 1FGL sources. Circles indicate the additional sources considered in our background model. **Panel (b):** Residual counts after the subtraction of the counts attributed to the background model. **Panel (c):** Residual counts after the subtraction of the counts attributed to the background model and to RX J1713.7–3946.

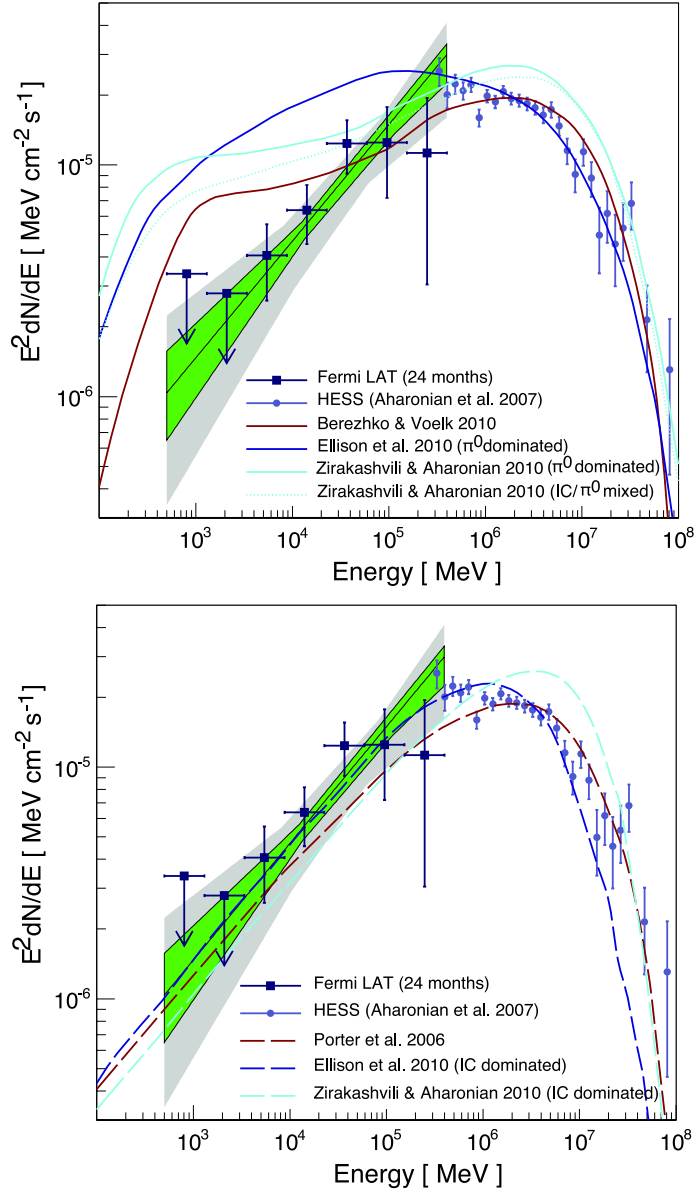


Fig. 3.— Energy spectrum of RX J1713.7–3946 in gamma rays. Shown is the *Fermi*-LAT detected emission in combination with the energy spectrum detected by H.E.S.S. (Aharonian et al. 2007). The green region shows the uncertainty band obtained from our maximum likelihood fit of the spectrum of RX J1713.7–3946 assuming a power-law between 500 MeV and 400 GeV for the default model of the region. The gray region depicts the systematic uncertainty of this fit obtained by variation of the background and source models. The black error bars correspond to independent fits of the flux of RX J1713.7–3946 in the respective energy bands. Upper limits are set at 95% confidence level. Also shown are curves that cover the range of models proposed for this object. These models have been generated to match the TeV emission and pre-date the LAT detection. The top panel features predictions assuming that the gamma-ray emission predominately originates from the interaction of protons with interstellar gas (brown: Berezhko & Völk (2008), blue: Ellison & Vladimirov (2008), cyan (solid/dashed): Zirakashvili & Aharonian (2010)). The bottom panel features models where the bulk of the gamma-ray emission arises from interactions of electrons with the interstellar radiation field (leptonic models). (brown: Porter et al. (2006), blue: Ellison & Vladimirov (2008), cyan: Zirakashvili & Aharonian (2010)). See text for a qualitative discussion of these models.

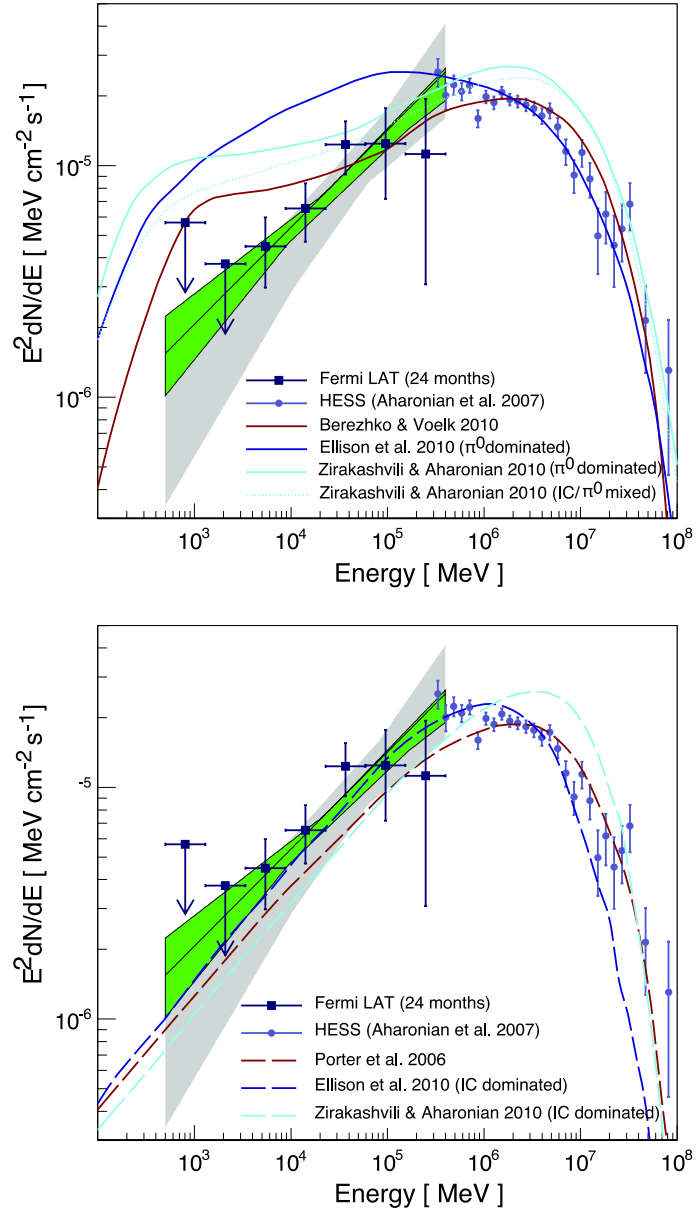


Fig. 4.— Same as Figure 3 but featuring the source and background model which resulted in the softest spectrum for RX J1713.7–3946 instead of our default model.

REFERENCES

420

421 Abdo, A. A., et al. 2010a, *ApJS*, 188, 405

422 Abdo, A. A., et al. 2010b, *ApJ*, 710, L92

423 Abdo, A. A., et al. 2010c, *Physical Review Letters*, 104, 101101

424 Abdo, A. A., et al., 2009a, *Phys. Rev. D*, 80, 122004

425 Abdo, A. A., et al. 2009b, *Astrophys. J.*, 696, 1084

426 Acero, F., et al., 2009, *A&A*, 505, 157

427 Aharonian, F., et al, 2006, *Astron. Astrophys.*, 449, 223

428 Aharonian, F., et al. 2007, *Astron. Astrophys.*, 464, 235

429 Albert, J., et al., 2007, *Astron. Astrophys.*, 474, 937

430 Atwood, W. B., et al. 2009, *ApJ*, 697, 1071

431 Baring, M. G., Ellison, D. C., Reynolds, S. P., Grenier, I. A. & Goret, P. 1999, *ApJ*, 513,
432 311

433 Bell, A. R. 1978, *Mon. Not. R. Astron. Soc.*, 182, 147

434 Berezhko, E. G. & Völk, H. J. 2008, *A&A*, 492, 695

435 —. 2010, *A&A*, 511, A34+

436 Blandford, R. D. & Ostriker, J. P. 1978, *Astrophys. J. Lett.*, 221, L29

437 Bykov, A. M., Uvarov, Y. A., & Ellison, D. C. 2008, *ApJ*, 689, L133

438 Cassam-Chenai, G., et al., 2004, *A&A*, 427, 199

439 Castro, D., & Slane, P. 2010, *ApJ*, 717, 372

440 Dame, T. M., Hartmann, D., & Thaddeus, P. 2001, *Astrophys. J.*, 547, 792

441 Drury, L., Aharonian, F. A., Malyshev, D., & Gabici, S. 2009, *A&A*, 496, 1

442 Ellison, D. C., Patnaude, D. J., Slane, P., & Raymond, J. 2010, *ApJ*, 712, 287

443 Ellison, D. C. & Eichler, D. 1984, *ApJ*, 286, 691

- 444 Ellison, D. C. & Vladimirov, A. 2008, *ApJ*, 673, L47
- 445 Fukui, Y., et al 2003, *PASJ*, 55, L61
- 446 Gotthelf, E. V., et al. 2001, *Astron. Astrophys. Lett.*, 552, L39
- 447 Green, D. A. 2004, *Bulletin of the Astronomical Society of India*, 32, 335
- 448 Hwang, U., et al. 2004, *Astrophys. J. Lett.*, 615, L117
- 449 Jones, F. C. & Ellison, D. C. 1991, *Space Sci. Rev.*, 58, 259
- 450 Katz, B. & Waxman, E. 2008, *Journal of Cosmology and Astro-Particle Physics*, 1, 18
- 451 Koyama, K., et al. 1997, *PASJ*, 49, L7
- 452 Lazendic, J. S., et al. 2004, *ApJ*, 602, 271
- 453 Malkov, M. A. 1999, *ApJ*, 511, L53
- 454 Malkov, M. A. & Drury, L. 2001, *Reports on Progress in Physics*, 64, 429
- 455 Mattox, J. R., et al., 1996, *ApJ*, 461, 396
- 456 Moriguchi, Y., et al. 2005, *ApJ*, 631, 947
- 457 Morlino, G., Amato, E., & Blasi, P. 2009, *MNRAS*, 392, 240
- 458 Pfeffermann, E. & Aschenbach, B. 1996, in *Roentgenstrahlung from the Universe*, 267–268
- 459 Pohl, M., Yan, H., & Lazarian, A. 2005, *ApJ*, 626, L101
- 460 Porter, T. A., Moskalenko, I. V., & Strong, A. W. 2006, *ApJ*, 648, L29
- 461 Rando, R. for the Fermi LAT Collaboration. 2009, [astro-ph/0907.0626](https://arxiv.org/abs/astro-ph/0907.0626)
- 462 Slane, P., et al. 1999, *ApJ*, 525, 357
- 463 Takahashi, T., et al., 2008, *PASJ*, 60, 131
- 464 Tanaka, T., et al. 2008, *ApJ*, 685, 988
- 465 Uchiyama, Y., Aharonian, F. A., & Takahashi, T. 2003, *A&A*, 400, 567
- 466 Uchiyama, Y., et al. 2007, *Nature*, 449, 576
- 467 Uchiyama, Y., Takahashi, T., & Aharonian, F. A. 2002, *PASJ*, 54, L73

- 468 Wang, Z. R., Qu, Q.-Y., & Chen, Y. 1997, *A&A*, 318, L59
469 Yamazaki, R., Kohri, K., & Katagiri, H. 2009, *A&A*, 495, 9
470 Zirakashvili, V. N. & Aharonian, F. A. 2010, *ApJ*, 708, 965